Chinese Chemical Letters 35 (2024) 109173

Contents lists available at ScienceDirect

Chinese Chemical Letters

journal homepage: www.elsevier.com/locate/cclet

Theoretical and experimental design in the study of sulfide-based solid-state battery and interfaces

Hongjie Xu[a,c], Yujie Su[a], Chenggong Zheng[a], Yuchen Wang[a], Yuping Tong[a], Zhongzheng Yang[a], Junhua Hu[b,*]

[a] School of Materials Science and Engineering, North China University of Water Resources and Electric Power, Zhengzhou 450046, China
[b] School of Materials Science and Engineering, Zhengzhou University, Zhengzhou 450001, China
[c] Henan Titanium Based Advanced Materials Industrial Research Institute, Jiaozuo 454191, China

ARTICLE INFO

Article history:
Received 29 July 2023
Revised 24 August 2023
Accepted 6 October 2023
Available online 7 October 2023

Keywords:
Theoretical simulation
Sulfide-based electrolytes
All solid-state battery
Cathode-electrolyte interface
Interface compatibility

ABSTRACT

In recent years, due to the increasing demand for portable electronic devices, rechargeable solid-state battery technology has developed rapidly. Lithium-ion batteries are the systems of choice, offering high energy density, flexible and lightweight design, and longer lifespan than comparable battery technologies. Therefore, a better understanding of the relationship between electrochemical mechanism and structural properties from theory and experiment will enable us to accelerate the development of high-performance and security batteries. This review discusses the interplay between theoretical calculation and experiment in the study of lithium ion battery materials. We introduce the application of theoretical calculation method in solid-state batteries through the combination of theory and experiment. We present the concept and assembly technology of solid-state batteries are reviewed. The basic parameters of solid-state electrolytes, especially sulfide-based solid-state electrolytes and their interface mechanisms with high-voltage cathode materials, are analyzed by theoretical methods. We present an overview on the scientific challenges, fundamental mechanisms, and design strategies for solid-state batteries, especially focusing on the issues of stability on solid-state electrolytes and the associated interfaces with both cathode and electrolyte. Owing to the theoretical models, we can not only reveal the unprecedented mechanism from the atomic scale, but also analyze the interface problems in the battery thoroughly, thus effectively designing more promising electrolyte and interface coating materials. It blazed a new trial for engineering an interphase with improved interfacial compatibility for a long-term cyclability.

1. Introduction

The worldwide revolution on decarbonization continues to drive the construction of renewable energy networks in modern life [1–3]. Compared with traditional ones, new energy sources account for an increasing proportion. However, the new energy must be applied through energy storage and conversion. Li-ion batteries (LIBs), as the predominant technology of electrochemical energy storage, have been expanded for deployment into emerging decarbonized areas [4–6]. Obviously, to obtain a higher energy density battery, it is inseparable from the lithium metal anode [7,8]. However, in traditional batteries, the organic liquid electrolyte (LE) used in contact with the metal lithium is easy to form lithium dendrites, which is a short circuit of the battery and causes safety problems [9,10]. As an essential component of solid state batteries (SSBs), solid electrolytes (SEs) overcome the shortcomings of liquid counterparts, such as low thermal stability, flammability, and leakage, thus playing a critical role for improved safety [11–14]. At the same time, it also further meets the development demand of specific capacity of electric vehicle in the market. Whereas, in order to achieve a wide range of market penetration and meet the market demand on the development of electric vehicles, it is urgent to exploit a new generation of energy storage devices with increasing energy density (>350 Wh/kg) and safety [15–17].

SSBs that employ a SEs instead of organic LE are the promising direction of battery development [14,18–21]. Besides, the resulting SSBs could offer substantially increased energy density by enabling the combination of high-specific-energy lithium metal anodes and prevalent high-voltage layered oxide cathodes [22]. In recent years, owing to the enormous advantages of SSBs, it has continuously set off exploratory boom in the field of new energy. However, there

* Corresponding author.
E-mail address: hujh@zzu.edu.cn (J. Hu).

https://doi.org/10.1016/j.cclet.2023.109173
1001-8417/

are still many factors that hinder its practical application. SEs are the key components of SSBs, and their intrinsic nature play a decisive role in the overall performance of SSBs. The properties of ideal SEs applied in SSBs should include (1) the high ionic conductivity greater than 1 mS/cm [23], (2) not sensitive to humidity, (3) great thermodynamic stability, (4) wide electrochemical window to accommodate both of the electrode [24,25], (5) electrically insulating to avoid self-discharging, and (6) appropriate stiffness and fracture toughness. At present, no SEs can meet all the above demands, which is also the first major challenge for SSB. At present, there are four categories of SEs that have been developed, mainly including oxides, halides, sulfides, polymer and composite solid electrolytes. Due to their bcc-like anion framework of sulfide-based electrolyte, it has been proven to be equipped with higher ion transport ability than the other electrolytes [26,27].

At present, the main sulfide solid electrolytes (SSEs) that have attracted people's research interest are as follows: $Li_7P_3S_{11}$ (LPS) (17 mS/cm), $Li_{10}GeP_2S_{12}$ (LGPS) (12 mS/cm), and $Li_{9.54}Si_{1.74}P_{1.44}S_{11.7}Cl_{0.3}$ (25 mS/cm) [28–30]. However, this electrolyte system generally has similar problems such as water sensitivity, narrow band gap, and incompatibility with metal lithium anodes and high-voltage cathodes materials [17,31–34]. The above problems result in the low capacity and cycle performance of sulfide-based SSB. In addition, owing to the serious solid-solid interface contact, internal grain boundaries and electrochemical reaction in the SSBs, the internal resistance between the electrode and the electrolyte has increased, which makes the SSBs have a higher polarization than LE cells [35]. Such issues are also related to the morphology and structural characterization of solid electrolytes. The SSEs with a narrow electrochemical window imply that its oxidation potential is low, and the electrolyte is easily decomposed into intermediate phase and the structure is destroyed during the electrochemical test. For example, the decomposition voltages of LGPS and LPS are low, which are 2.15 V and 2.41 V, respectively [36].

Furthermore, due to the chemical potential incompatibility of SSEs with cathode/anode materials, the internal interface of the battery is unstable during the cycle. Such reactions will form a detrimental anode–electrolyte interphases (AEI) and undesirable electrolyte-cathode interphases (CEI), thereby hindering the diffusion and charge transfer of lithium ions inside the SSBs [37,38]. Aiming at the complex interface problems in SSBs, both theoretical calculations and experimental methods can be applied. Density functional theory (DFT) calculations and molecular dynamics simulations can analyze the interface mechanism from thermodynamic and kinetic stability and microscopic interactions between atoms. For example, the combination of $LiCoO_2$ (LCO) and SSEs is thermodynamically unstable at high voltage, and it is easy to react to form Li_xP and Li_xS at the interface [39,40]. Through calculation, it is found that $Li_{10}GeP_2S_{12}$ and Li_6PS_5Cl are unstable with Li [41,42]. Meanwhile, a large number of experimental work has also exposed the interface problem between the electrode and sulfide electrolyte in the solid-state battery [43–48]. There is a good contact area of the ion transport pathway between the cathode and the electrolyte, which leads to high capacity and energy density of the lithium battery. In general, the main interface problem is due to the poor mechanical contact of the cathode/sulfide, since the volume change is caused by the repeated shrinkage/expansion of the active cathode material during the long-term charge and discharge process [22]. Similarly, the instability of the cathode/SEs interface involves poor oxidation side reactions between the cathode and metal sulfides electrolyte due to electrochemical incompatibility, as well as interface aging/evolution during the long-term cycle of the battery [49].

Typically, in-depth analysis of complex interfacial engineering requires advanced characterization techniques, such as *in-situ* XPS, nuclear magnetic resonance (NMR), *in-situ* Raman and cryo-electron microscopy [50]. Recently, some groups have proposed the use of time-of-flight secondary ion mass spectrometer (TOF-SIMS) to study the surface and interface information [51]. In addition, researchers have also tried to develop computational simulation of interface morphology, analyzed the reaction mechanism between cathode/SEs, and then made up for the defects in the experimental process. The combination of theory and experiment can deeply explore the thermodynamic and kinetic reaction processes inside the interface, and more effectively propose interface protection strategies [52]. The application of theoretical calculations in SSBs is shown in Fig. 1.

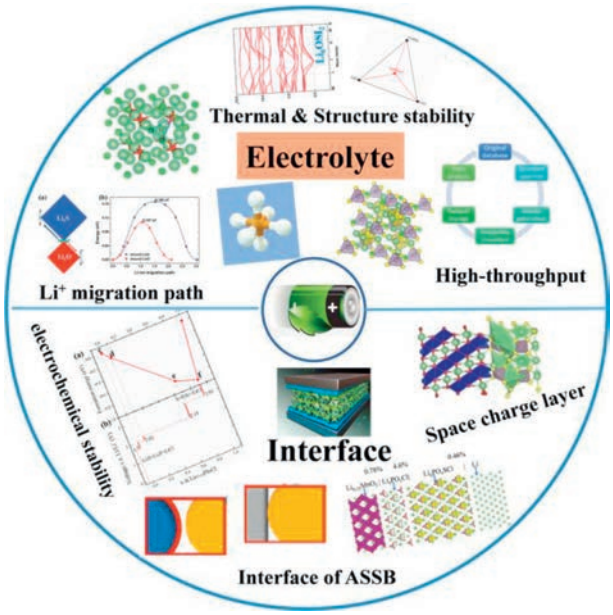

Fig. 1. The application of theoretical calculations in SSB. Reprinted with permission [42]. Copyright 2021, Wiley. Reprinted with permission [53]. Copyright 2016, Chinese Physical Society and IOP Publishing Ltd.

Since high energy and safety are the direction of battery research, the focus of this work is to analyze the key of materials in SSBs, pay attention to the interface problems in battery, and propose effective solutions for interface design. Some reviews summarize the development of electrolyte materials and the optimization technology of battery assembly, but rarely discuss the application and research progress of theoretical simulation in SSBs [25,41,53–64]. Here, we primarily focus on the preparation technology of SSBs, especially the assembly of SSBs with metal sulfides as solid electrolyte, because that sulfides exhibit outstanding battery performance and can maintain the SSBs cycle without adding LE. Secondly, we present the fundamental understanding of the establishment of the interface model between the sulfide SEs and the cathode in SSBs and the reaction mechanism, existing challenges and potential solutions. Finally, we propose an effective strategy to alleviate the interface problem by using coating materials. The recent application of high-throughput calculation methods in the design of new coating materials is discussed. Combined with experimental research, it is further verified that coating materials can effectively alleviate the incompatibility between interfaces. At the same time, the relationship between the materials' properties and phase structure was discussed by combining electrochemical characterization, physical phase, and morphology characterization. A deeper understanding of the mechanism of SSBs provides guidance for us to develop new SEs and interface modification materials. The information can promote the practical application of interface engineering and make it possible to assemble high-energy SSBs.

2. Solid-state battery technologies

2.1. State-of-the-art solid-state batteries

Compared with the traditional flammable LE, the SEs may also give additional mechanical stability to slow down the dendrite growth in the alkali metal anode. Table 1 lists the recent development status of sulfide-based SSBs [27,42,65–70]. Although the addition of a small amount of LE between the electrolyte and the electrode interface in the SSB can enhance the cycle performance of the battery to a limited extent, it does not fundamentally solve the interface problem in the battery. Moreover, this solid-liquid mixed battery assembly method cannot be clearly defined as a solid-state battery in the whole sense. In some literatures, solid-state batteries are defined as "*quasi*-solid", "mixed solid" or "semi-solid" batteries according to the amount of LE added [64]. Since the battery performance appears differently due to the addition of LE, this description may arise controversy. Therefore, we classify the battery through the way whether it contains liquid to avoid confusion (Fig. 2): (1) Liquid electrolyte battery. Such LIBs are mainly composed of electrodes, separators and liquid electrolytes. The LE is mainly composed of two categories: aqueous and nonaqueous electrolytes. For the gel electrolyte, the gel polymer is added to LE, thereby improving the plasticity and mechanical strength of the electrolyte, while the transmission of lithium ions only occurs in the liquid phase. (2) Semi-solid battery. In order to alleviate the interface problem in the LIBs, the solid-liquid mixing method is used as the electrolyte, and the expression of the semi-solid battery is proposed. (3) All-solid-state battery (ASSBs). This type of LIBs completely uses SEs as the transmission medium of Li^+, such as inorganic SSBs, polymer SSBs.

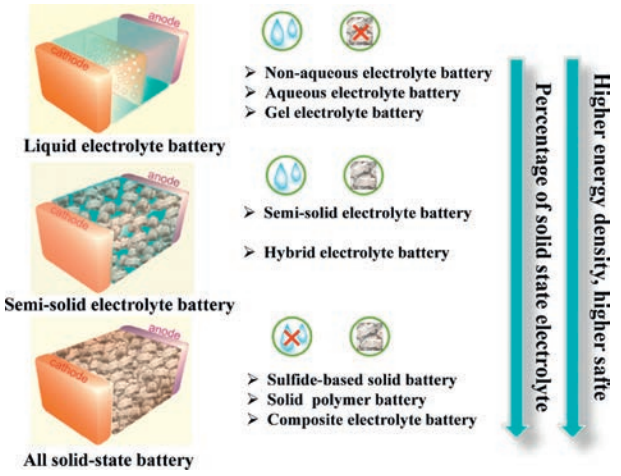

Fig. 2. Schematic illustration of the classifications of prevailing lithium ion batteries. According to the amount of liquid added, the battery type is divided into three types. Reprinted with permission [64]. Copyright 2020, American Chemical Society.

2.2. All solid-state batteries and assembly

Based on the various advantages performed by sulfide-based solid electrolytes, a series of follow-up studies on the exploratory synthesis of their derivatives have been initiated. Consequently, the sulfide solid electrolytes family has grown substantially and can be classified into five types in light of crystalline state and specific crystal structure, including glasses [71,72], glass-ceramic [73,74], thio-LISICON [75–77], LGPS-type [29,78–81], and argyrodite-type [82–85]. In the experiment, the synthesis process of SSEs with different crystal structures is similar to Fig. 3a, and each step needs to be operated in an inert gas [68]. At present, there are three types of processes for assembling ASSBs using SSEs (Figs. 3b–d). Each assembly technology has advantages and deficiencies. The method of hot pressing is safe with great voltage compatibility, while the interface contact is in an unfavorable position. The overall pressurized battery is featured with high ionic conductivity and interface contact, except for the vulnerability of the leak in the air. The technology of roll to roll has good flexibility, but short circuit is more likely to appear in the process.

2.3. Challenges in ASSBs

Although, ASSBs are well-performed, there is still a long distance from the actual industrial application [11,86]. In order to explore the potential mechanism in the above problems, thorough research have been carried on [14,31,87,88]. The challenges that need to be overcome in ASSBs include persistent interfacial adverse reactions, limited electrochemical windows, surface/interface physical contact problems, easy decomposition of exposed humid air, and crack or pulverization issues [35,89]. The sulfide-based SSBs with better performance should have advantages as follows: (1) During the charge-discharge cycle, the volume change of any part of the battery system is small; (2) The low interfacial stress is attributed to the ductility of the electrolyte and the sufficient compatibility between the interface phases for small lattice; (3) There is no harmful interfacial reaction in the formation of insulating phase or inhomogeneous interfacial phase layer; (4) High cross-interface bonding; (5) Voltage platform matching between positive and negative electrode materials; (6) Remarkable ion transport ability between positive and negative electrode materials; (7) The electrode should be endowed with great conductivity. The con-

Table 1
Performance of reported SSBs with metal sulfide-based electrolyte.

Year	Initial capacity (mAh/g)	Cycle performance	Conductivity (S/cm)	Battery configuration	Classification	Ref.
2022	600	80.8% retention after 500 cycles, 200 mA/g at 0.3 C and 60 °C	$\sim10^{-3}$	PMTH/Li_6PS_5Cl/Li−In	All solid-state battery	[65]
2023	600	77.5% retention after 2500 cycles at 0.5 A/g, 1–3 V and 25 °C	6.2×10^{-3}	a-$NbS_{4.5}$/20% super P@15% $Li_7P_3S_{11}$/$Li_{10}GeP_2S_{12}$ + Li_2S-24% P_2S_5–1% P_2O_5/Li	All solid-state battery	[66]
2022	200.7	87% retention after 500 cycles	1.54×10^{-3}	NCM88-S/Li_6PS_5Cl/$Li_4Ti_5O_{12}$	All solid-state battery	[67]
2021	188.4	74.45% retention after 210 cycles	3.17×10^{-3}	LCO@LNO/$Li_{3.875}Sn_{0.875}As_{0.125}S_4$/LTO	All solid-state battery	[68]
2023	256	90.1 mAh/g at the 50th cycle	2.45	(AQ)/$Li_7P_3S_{11}$/$Li_{1.5}BP_3DME_{10}$	Solid-state battery	[69]
2022	151.9	60% of the capacity after 450 cycles at 0.1 C	2.8	Li-$Li_{6.25}PS_4O_{1.25}Cl_{0.75}$-$LiCoO_2$	All solid-state battery	[42]
2023	101.0	Capacity retention of 94.8% after 1000 cycles at 1 C	12×10^{-3}	$LiNbO_3$@$LiCoO_2$/LiF@$Li_{10}GeP_2S_{12}$/Li	All solid-state battery	[70]
2023	550.00	550.00 mAh/g at 0.5 A/g after 1000 cycles	0.17	Li/Li_6PS_5Cl/MoS_6-CNT20@15%$Li_7P_3S_{11}$	All solid-state battery	[27]

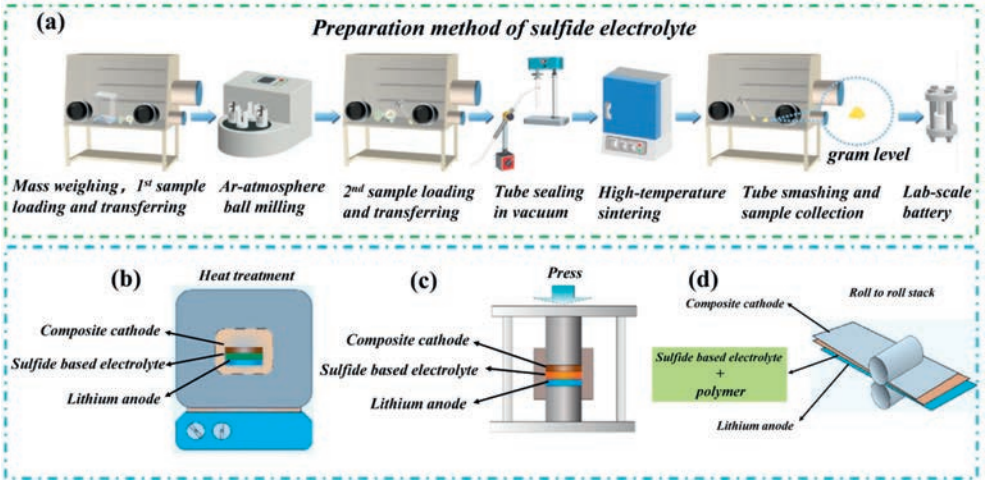

Fig. 3. (a) The synthesis processes of solid-phase method. Reprinted with permission [68]. Copyright 2021, Wiley. (b-d) Different types of assembly methods in ASSBs. Reprinted with permission [64]. Copyright 2020, American Chemical Society.

struction of ASSB with excellent performance is an important goal of our research, and also establish foundation for the industrialization of ASSB [42,68].

3. Theoretical computation of sulfide based solid-state electrolytes

At the end of the 19th century, with the continuous exploration of the microscopic world, the shortcomings of classical theory were gradually discovered. In order to more accurately study the electrons and atoms in the microscopic world, physicists created quantum mechanics in the 20th century. Quantum mechanics can accurately explain and describe all the basic interactions except the gravity described by general relativity. The Schrödinger equation used to explain wave mechanics and quantum mechanics can simplify the multi-electron system into a single-electron system for processing. The Schrödinger equation is established based on the variation of the state of the particles with time. The first-principles calculation method based on density functional theory (DFT) solves the problem of solving multi-particle Schrödinger equation. The multi-body problem is transformed into a simple single-body problem. The accuracy of DFT is dependent upon the exchange-correlation (XC) functionals, which involves approximations.

This review discusses the interaction between theoretical calculation and experiment in the design of new materials for batteries, accelerating the prediction and development of advanced materials. The theoretical calculation method is mainly based on the first principle of DFT. Theoretical simulation in the field of energy storage materials and the calculation methods are mostly microscopic simulation at the atomic or molecular level. In order to accurately evaluate the overall performance of the battery, macroscale simulation is essential to describe all components of the battery as a whole, which is conductive to promote a new field of high-throughput battery system design. The properties of battery materials that can be calculated at present and the corresponding calculation methods for simulation (Fig. 4) [90].

The main calculation methods commonly used are *ab initio* molecular dynamics (AIMD), molecular dynamics (MD), climbing image nudged elastic band (CI-NEB), and alloy-theoretic automated toolkit (ATAT). It has been shown that the activation energies from AIMD and CI-NEB often agree well, as long as the identified pathways from the latter are dominant in the statistic process typically experienced in a molecular dynamic process. MD molecular dynamics is a calculation method based on Newton mechanics to

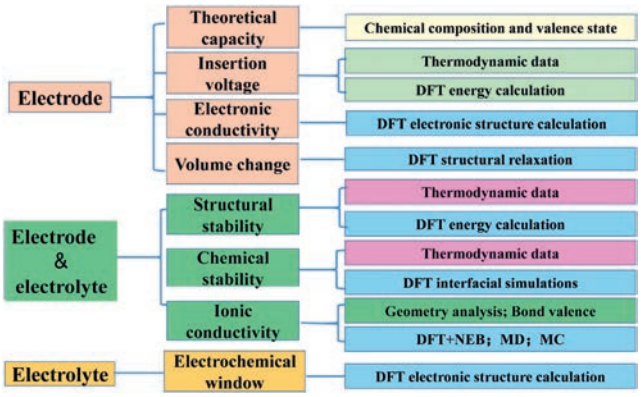

Fig. 4. Calculation method of key materials in solid-state batteries. Reprinted with permission [90]. Copyright 2016, Chinese Physical Society.

simulate the interaction and motion between molecules, without considering the interaction between electrons. ATAT is a generic name that refers to a collection of alloy theory tools developed by Axel van de Walle, in collaboration with various research groups. The most stable phase and the lowest energy structure of each component phase can be determined by using ATAT. The comparison between different calculation methods is shown in Table 2.

3.1. Ion diffusion mechanism

The ionic conductivity is dictated by long-range diffusion, which usually follows an Arrhenius form of relationship. First-principles *ab initio* molecular dynamics (AIMD) [91,92] is then carried out to study the ionic transport behavior of Li ions at elevated temperatures, thus providing further insights through statistic processes. In recent works, AIMD explains the transport mechanism of lithium ions by counting the diffusion distance of lithium ions in the electrolyte system at different times. In the process of data statistics, the influence of errors caused by periodic boundary conditions on the actual MSD is considered and corrected. Thus, the assessment of diffusion coefficient D for Li^+ ions by AIMD simulation at elevated temperatures can be extracted *via* Eq. 1.

$$D = \frac{1}{2dt} < [\Delta r(t)]^2 > \quad (1)$$

which is obtained through the average mean square displacement (MSD) $\langle[\Delta r(t)]^2\rangle$ from molecular dynamics (MD) runs at each tem-

Table 2
The comparison between different calculation methods.

Calculation method	Application in lithium battery	Advantages	Disadvantages
AIMD	Ionic transport capacity Diffusion activation energy	Accuracy	Large amount of calculation; Time-consuming; The number of atoms in the calculated system is less than 100
MD	Calculate the motion of molecules, ion, and clusters	A large number of single atoms or molecules can be calculated	Inaccuracy
CINEB	Showing an ion migration path	Visualization of energy changes during ion movement	The initial state and final state are not easy to be determined in the calculation process
ATAT	Is a generic name that refers to a collection of alloy theory tools	By calculating the energy of the system, various properties of the structure are obtained (oxidation/reduction potential, voltage platform, volume change, *etc.*)	Large amount of calculation; Time-consuming

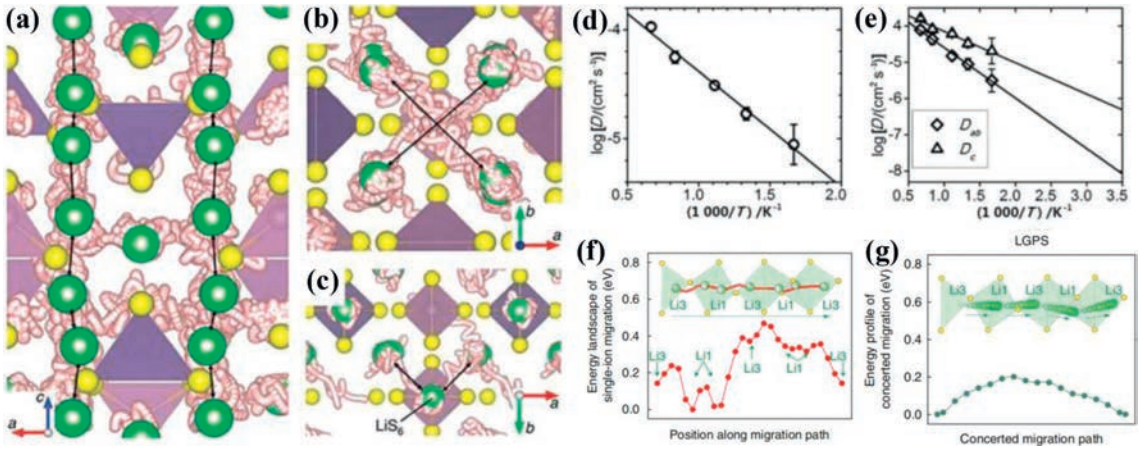

Fig. 5. (a-e) The Arrhenius plot of the d overall diffusion coefficient and the diffusion coefficient in the *c* direction D_c and e in the *ab* plane D_{ab}. Reprinted with permission [95]. Copyright 2012, American Chemical Society. (f) The energy change of a single Li^+ diffusion along the *c*-axis direction. (g) The migration energy of Li^+ in LGPS diffuses along the *c* direction to the next site. Reprinted with permission [93]. Copyright 2017, Springer Nature.

perature *T* over a period of time *t*. And *d* is the dimensionality factor. Using the Arrhenius relation,

$$D = D_0 \exp\left(-\frac{E_a}{k_B T}\right) \tag{2}$$

the ionic conductivity σ can be derived using the Nernst-Einstein equation,

$$\begin{aligned} \sigma &= \frac{\rho z^2 F^2}{RT} \\ D &= \frac{\rho z^2 F^2}{RT} D_0 \exp\left(-\frac{E_a}{k_B T}\right) \\ &= \frac{A_0}{T} \exp\left(-\frac{E_a}{k_B T}\right) \end{aligned} \tag{3}$$

where ρ is the molar density of diffusing alkali ions in the unit cell, *z* is the charge of alkali ions (+1 for Li^+), *F* and *R* are the Faraday's constant and the gas constant, respectively, D_0 is a constant, E_a is activation energy for diffusion, k_B is the Boltzmann constant, and $A_0 = \rho z^2 F^2 D_0 / R$.

AIMD can simulate the actual diffusion path of ions and analyze the diffusion mechanism, so a visual ion migration process can be obtained, which can be used as input for the nudged elastic band (NEB) method (Fig. 5) [93,94]. AIMD cannot only simulate the actual diffusion mechanism of atoms, but also visualize the ion migration path. Mo *et al*. employed AIMD simulation to confirm fast Li diffusion in a 1D diffusion channel along the *c* direction of $Li_{10}GeP_2S_{12}$ (LGPS) but also predicted two additional diffusion pathways in the *ab* plane (Figs. 5a–c) [95]. The diffusion coefficient *D* reveals the effective path of Li^+ diffusion, so the diffusion efficiency along the *c*-axis direction is higher. The ionic conductivity of alkali metals is obtained from the diffusion coefficient by the Nernst-Einstein equation. The diffusion coefficients of LGPS from 600 K to 1500 K are given (Figs. 5d and e). The calculated ionic conductivity at room temperature is as high as 9 mS/cm, and the overall activation energy barrier is about 0.21 eV, which is consistent with the experimental results. From the perspective of material design, AIMD is an effective means to predict the transport properties of lithium ions below room temperature by high temperature diffusion data (Figs. 5f and g). The emergence of LGPS has aroused great interest among energy storage researchers, so that more and more efforts have been made to study the replacement of expensive Ge elements so as to obtain better ionic conductivity [79–81].

3.2. Electrochemical window

For inorganic electrolyte, it is very essential to have a wide electrochemical window. It can be obtained not only by testing, but also by DFT analyzing the thermodynamic properties, and then calculate the electrochemical window value [96]. An overall assessment of change of configurational energy for a SEs with respect to content of lithium ion, *x*, can be established through energy minimization, for example, using ATAT [97,98]. Ceder *et al*. calculated the electrochemical windows of different components of SE (Fig. 6a) [99]. It shown that the stability of different types of electrolytes has been determined by their binary phase, or in the case of mixed anion materials. Therefore, $Li_{1.3}Al_{0.3}Ti_{1.7}(PO_4)_3$ exhibits high oxidation performance due to the formation of strong covalent bonds between P and O [31]. The oxidation potential of the sulfide electrolyte is poor, which is mainly related to the S^{2-} in the binary phase Li_2S. The electrochemical window of Li_6PS_5Cl

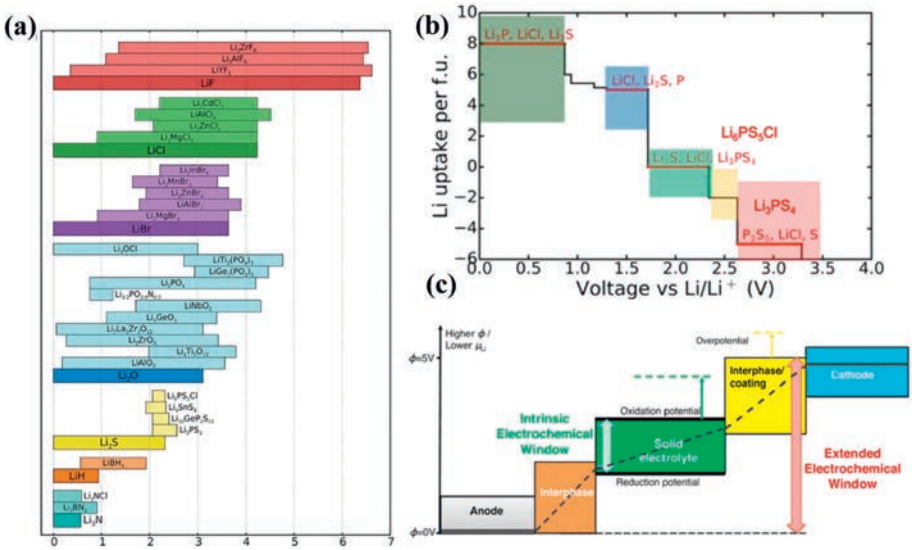

Fig. 6. (a) The electrochemical window of SE with different components. Reprinted with permission [99]. Copyright 2016, American Chemical Society. (b) The phase diagram of LPSCl at different voltages shows a stable voltage range of 1.7–2.3 V. Reprinted with permission [31]. Copyright 2020, American Chemical Society. (c) Describe the nature and practical testing electrochemical window diagram in SE. Reprinted with permission [100]. Copyright 2015, American Chemical Society.

(LPSCl) is shown in Fig. 6b [31]. It can be seen that LPSCl is about at 1.7 V, while LPSCl is oxidized above 2.3 V, and its stable electrochemical window is only 1.7–2.3 V.

The voltage window calculated by the theoretical calculation is not completely consistent with the experimental results (Fig. 6c) [100]. In fact, the difference between the initial potential and the electrochemical window observed in the experiment is mainly due to the difference in the chemical potential of Li between the intermediate phase as well as the electrolyte and the electrode. The valid electrochemical window of SE not only includes the intrinsic electrochemical window of SE, but also the electrochemical window of the interphases. Therefore, in the design process of new electrolytes, we should pay attention to the (de)lithiation redox potential of SSEs.

3.3. Electrochemical stability

The electrochemical stability of the SE is directly related to the integrative performance of the battery. It was verified with galvanostatic intermittent titration technique (GITT) analysis, electrochemical charge/discharge profiles, cyclic voltammetry (CV) and other electrochemical techniques in the experiment. DFT can explain the thermodynamic stability of the electrolyte and analyze the electrochemical stability of SE by energy calculation (Fig. 7).

When an ion migrates from state A to state B, the average electrochemical potential $V_{A\text{-}B}$, for the transition between state A ($Ak_x\prod$) and state B ($Ak_{x+\Delta x}\prod$), with reference to electrochemical potential *vs.* alkali Ak related to total energies (E_{total}) can be calculated as follows [101,102]:

$$V_{A-B} = \frac{1}{z}\left\{\left[E_{total}\left(Ak_{x+\Delta x}\prod\right) - E_{total}\left(Ak_x\prod\right)\right]/\Delta x - E_{total}(Ak)\right\} \quad (4)$$

where x is the number of alkalis in the formula unit of $Ak_x\prod$, charge value $z=1$ for alkali ion, Δx is the difference value of alkali atoms, and $\prod$ refers to the collection of other constituents. For SSEs, with the change of lithium content, the corresponding decomposition phase and electrochemical potential are different, and the difference of voltage plateau between two adjacent states is the corresponding electrochemical platform, (Figs. 7a and b) [42].

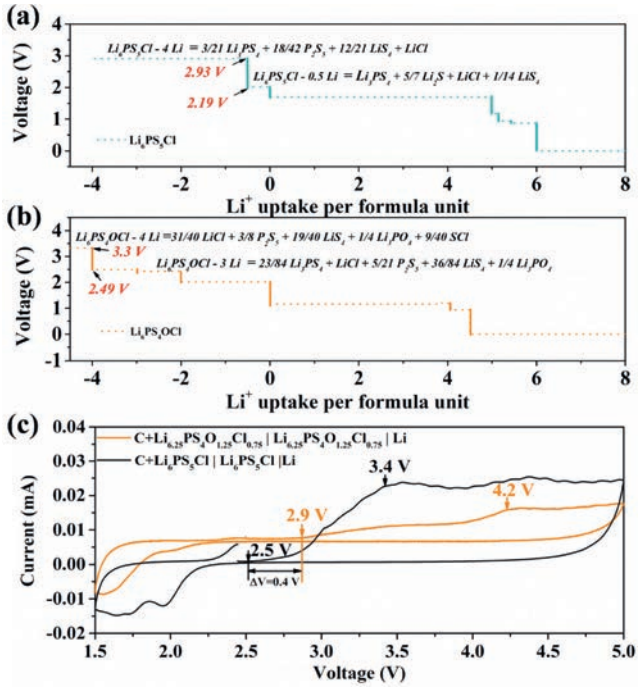

Fig. 7. The electrochemical windows of electrolytes with different compositions are calculated theoretically: (a) Li_6PS_5Cl and (b) Li_6PS_4OCl against stable constituent phases. (c) Experimental cyclic voltammetry (CV) tests for the battery. Reprinted with permission [42]. Copyright 2022, Wiley.

This is consistent with the oxidation potential and reduction potential of the sulfide electrolyte obtained by CV test (Fig. 7c).

4. Cathode-SSEs interface

The electrochemical performance of cathode matching different SSEs in ASSBs is quite obvious, and its internal mechanism is still unclear. Since the interface products are embedded in the composite cathode, it is difficult to characterize and accurately quantify the interface and products, which greatly limits the study of the interface reaction mechanism. In this part, we focus on the analy-

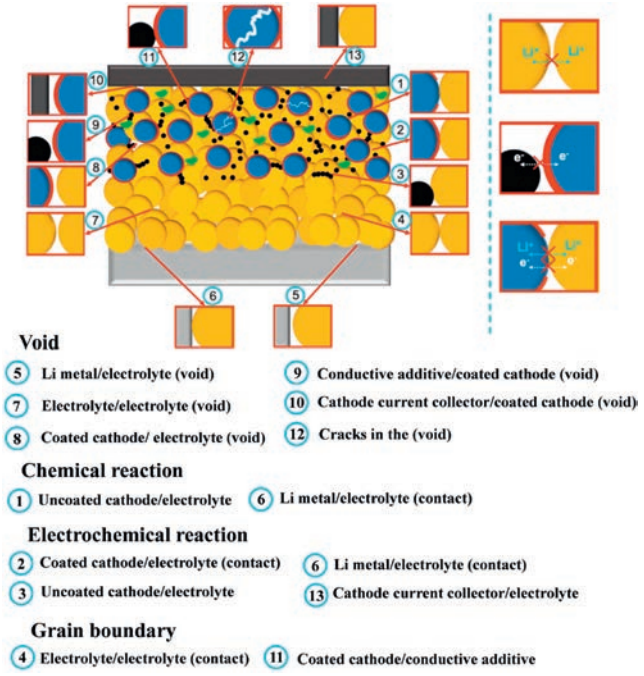

Fig. 8. Schematic illustration of interfacial phenomena experienced in ASSBs. Reprinted with permission [31]. Copyright 2020, American Chemical Society.

sis of the interface between SSEs and cathode by establishing theoretical interface model and experiment.

Compared with LE batteries, most ASSBs have serious polarization, poor capacity, as well as inferior power and cycle ability, which is not only related to the properties of each component, but also attributed to serious interface problems [35]. The interface contact, internal grain boundaries, and chemical and electrochemical reactions all lead to an increase in the interfacial resistance between the various parts of the battery (Fig. 8) [31].

The battery mentioned above is mainly composed of anode, cathode and electrolytes. The properties of each component and the interaction between them have a significant influence on the integrated performance of the battery [36–38]. Diverse types of electrolytes should be selected to match the appropriate cathode to achieve the best ASSB properties. In the system of sulfide SE assembled ASSB, the use of cathode materials with high oxidation potential is the key to achieve high energy density ASSBs [20,21,103]. However, the poor compatibility of sulfide electrolyte with high voltage cathode materials such as LCO, $LiNi_aCo_bMn_{(1-a-b)}O_2$, $LiNiO_2$ and olivine $LiFePO_4$ has brought about electrochemical incompatibility at the interface. Therefore, how to control and design the interface in ASSB has become a critical problem in recent years.

4.1. Inerface stability

Since the liquid electrolyte is easy to diffuse through the porous electrode and wet the electrode surface, a surface-to-surface contact is formed between the SSEs and the electrode material with irregular particle shape, while the SSEs as a granular contact with the granular electrode material will form hole and point-point contact, which is unfavorable to the transport of Li^+ at the interface. Hertz *et al*. has used two elastic spheres to simulate the point-to-point contact between balls [104]. In the interior of the solid-state battery, the holes and poor contact surfaces that original existed in the electrode-SSEs will further deteriorate under the action of the electric field. Xu *et al*. calculated the comprehensive performance of common commercial cathode materials by first-principles. It was found that most electrode materials shall undergo phase transition, lattice expansion/contraction or structural changes during the deintercalation of lithium, resulting in volume changes after charge and discharge [87–89].

In order to further research the interface reaction mechanism in ASSBs, not only some efforts have been made in theoretical simulation [34,98], but also effective strategies have been proposed during the experiment [30,33,38]. Although, the soft nature of the SSEs, the pressure applied when assembling the battery alone is not enough to make SEs contact closely with cathode. Many work reports that maintaining a certain pressure during the charge and discharge cycle is contribute to improve the overall performance of the ASSBs. However, the choice of pressure should be appropriate, because the lower pressure will affect the interface contact, the larger one will induce the rupture of the electrolyte piece, and even cause the short circuit of ASSBs [99,100]. Even if pressurization has improved the battery performance of sulfide electrolytes, it may not be effective for other types of electrolytes. Therefore, a more effective interface solution is needed in the following content.

4.2. Interface space charge layer

It is noticeable that the factors affecting the stability of the interface are also the space charge layer (SCL) formed by the battery during charging and discharging. Theoretically, all SEs/electrode interfaces possess SCLs. Yoshitaka *et al*. theoretically simulated the interface between LCO and Li_3PS_4 (LPS) and found that LCO decomposed into CoO_6 during the cycle, and lithium was adsorbed on the O site of the CoO_6 octahedron, resulting in the formation of SCL [105–107].

Haruyama *et al*. [108] firstly studied the most representative LCO/LPS and LCO/$LiNbO_3$/LPS interfaces in ASS-LIB composed of oxide cathode/sulfide electrolyte by DFT+U calculation combined with systematic solid-solid interface matching method and clarified the SCL mechanism and the influence of buffer layer on these interfaces (Fig. 9a). Recently, Xu *et al*. used Raman and TEM characterization techniques to visualize the reaction at the LCO/$Li_{6.25}PS_{5.25}Cl_{0.75}$ interface (Figs. 9b–h). It presented that the interface of LCO/ $Li_{6.25}PS_4O_{1.25}Cl_{0.75}$ (LPSOC) will form Li_3PO_4 *in situ* during charging and discharging, and the ionic conductivity of Li_3PO_4 is poor, which will affect the overall performance of the battery.

4.3. Chemical and electrochemical stability

The prediction in the performance of battery materials is mostly based on energy calculation. Ceder *et al*. researched the electrochemical stability of cathode/SSEs by DFT and calculated the reaction energy of various cathode/SEs interfaces (Fig. 10a) [99]. It can be seen from that the SEs with lower reaction energy with the cathode exhibits better stability. In general, the reaction energy between oxide electrolyte and cathode is lower than that of SEs. Thiophosphate materials often have high reaction energy, which is mainly due to the strong reaction between PS_4 group and oxide cathode, forming PO_4 group and transition metal sulfide. Mo *et al*. calculated the thermodynamic stability of a series of SSEs with four different cathodes in charged and discharged states (Figs. 10b and c) [109]. Through thermodynamic analysis illustrated that the stability between the cathode and SEs is related to the change of Li content and cation, and the change of chemistries is related to the anion type of both.

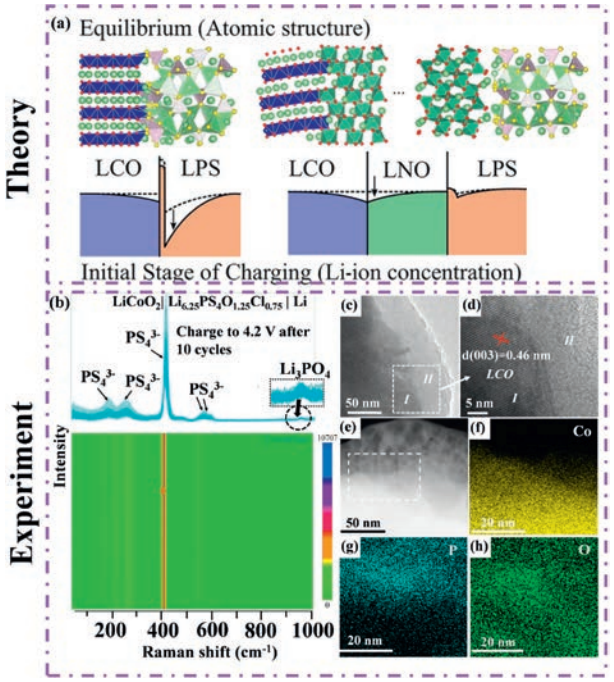

Fig. 9. (a) The change between cathode and SEs before and after charging at atomic scale. Reprinted with permission [108]. Copyright 2014, American Chemical Society. Characterization of the LCO|LPSOC interface in ASSB: (b) Raman test at the LCO|LPSOC interface. Reprinted with permission [42]. Copyright 2022, Wiley. (c-h) TEM test and HRTEM image of at the LCO|LPSOC interface. Reprinted with permission [42]. Copyright 2022, Wiley.

4.4. Artificial interface buffer layer

Up to now, investigators have proposed to introduce a buffer layer material between the cathode and SEs, which can effectively alleviate the above interface problems. The buffer layer material introduced should have the following characteristics: (1) excellent ionic conductivity; (2) Stable physical and chemical properties; and (3) a high oxidation potential.

Such a buffer layer material can prevent the electrolyte from contacting directly with cathode and reduce the occurrence of interfacial side reactions. For instance, using SSEs and $LiNbO_3$-coated LCO as a composite cathode to assemble battery, the system can improve the rate performance [110–112]. Most of the coatings have good chemical stability with the cathode and SSEs, thereby the original highly active interface can be converted into a more stable interface [113].

However, the coating technology mainly utilizes the favorable chemical/electrochemical reaction between coating and SEs, so it is important to select the matching coating materials for different SEs. Not all coating materials can improve the cycle performance of ASSB. For different electrolyte systems, it is necessary to select a suitable coating. At present, the development of most coating materials still reliant on trial-and-error approaches, which takes a long time. Therefore, Yang *et al.* proposed a specific high-throughput screening scheme to filter the functional materials by comprehensively evaluating their functionality (Fig. 11a). Hierarchical screening of 48 coating materials with optimal properties was carried out. Ceder *et al.* used a high-throughput search for suitable materials for cathode coatings in ASSBs [114]. In addition, Cao *et al.* reported that an amorphous $Li_{0.35}La_{0.5}Sr_{0.05}TiO_3$ (LLSTO) coating stabilized the interface between $LiNi_{1/3}Mn_{1/3}Co_{1/3}O$ (NMC)

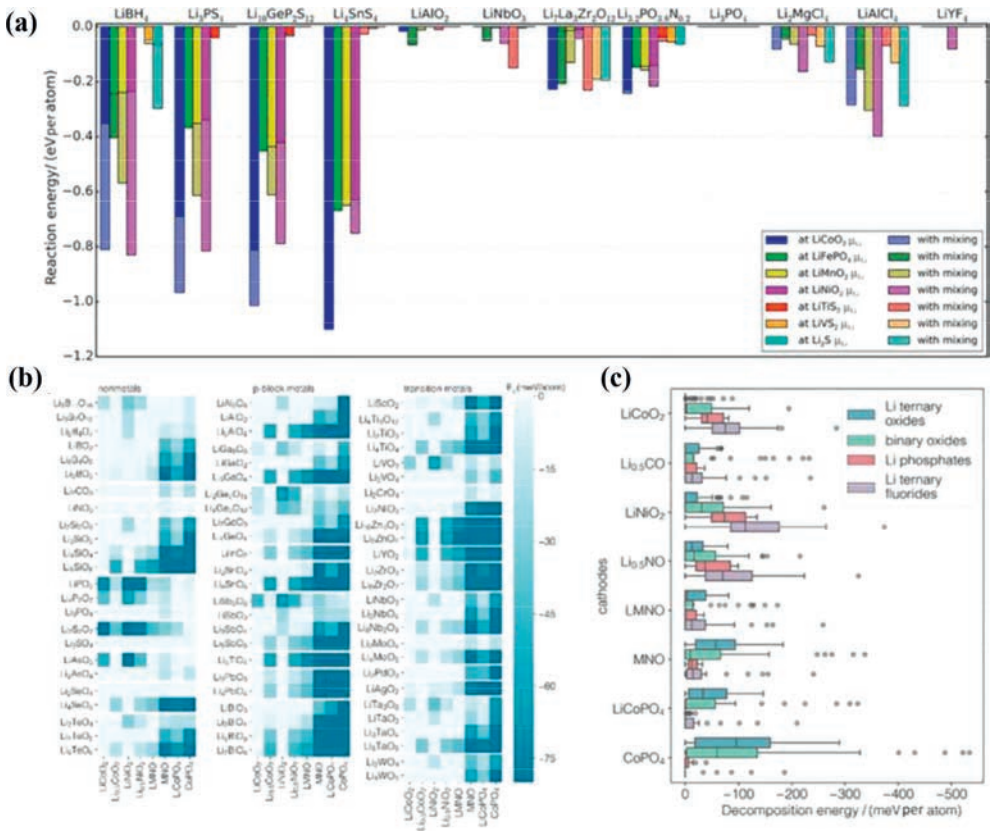

Fig. 10. (a) Calculation of interfacial reaction energy for different cathode/electrolyte combinations. Reprinted with permission [99]. Copyright 2015, American Chemical Society. (b) Calculation of decomposition energy of different lithium oxides. Reprinted with permission [109]. Copyright 2019, American Chemical Society. (c) Columnar diagram of decomposition energy of all cathode materials. Reprinted with permission [109]. Copyright 2019, American Chemical Society.

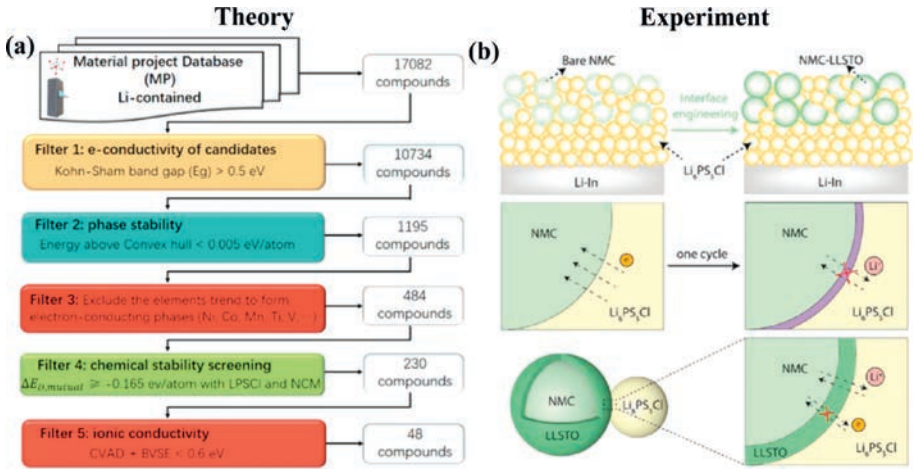

Fig. 11. (a) The flowchart of screening the coatings. Reprinted with permission [113]. Copyright 2023, Royal Society of Chemistry. (b) Schematic of a configuration of ASLBs with/without interface engineering. Reprinted with permission [115]. Copyright 2020, American Chemical Society.

and Li_6PS_5Cl in ASSBs [115]. A schematic of the stabilization mechanism of the LLSTO layer is shown in Fig. 11b. In short, the calculation provides a strong support for the selection of the interfacial coating materials, which can correctly guide the experiment, facilitating the high performance ASSBs with long-term cycling.

5. Conclusion and prospects

In this review, we firstly introduce the types of all-solid-state batteries and the latest assembly techniques. Then, the key performance parameters of sulfide electrolytes in ASSBs, including ionic conductivity and electrochemical stability, are analyzed by theoretical simulation and experiments. The interface problems in ASSBs are also discussed, mainly including the stability of the interface between SSEs and electrode, space charge layer, chemical and electrochemical stability. Finally, this review proposes an effective strategy for the interface problem in ASSBs, that is, using the coating material to block the cathode and electrolyte interface to improve the overall performance of the battery. At the same time, the latest progress of theoretical calculation in the interface problem of ASSBs and the screening of interface coating materials is also introduced. Theoretical computations have gradually begun to be widely used in the development and design of new energy materials, but some deficiencies still exist. So far, a large number of theoretical simulations on advanced materials have focused on solids crystals, while the amorphous polymer electrolytes and the interface with electrodes are not simulated enough.

Although theoretical calculations provide a visual interface model for the interface and have a more intuitive understanding of the hidden interface, these simulations still rely on the energy and bulk phase properties of the materials. However, the microstructure, crystal state and defects of the material and interface in the electrochemical state are not the same. Simply relying on a calculation method cannot accurately analyze the interface problems hidden in the battery. The ASSBs is a complex phase system involving chemical-electrochemical-physical-material surface, interface and other behaviors. Therefore, more efforts need to be done to develop new models and methods to achieve a more accurate simulation of the real situation of ASSBs materials and interfaces, combined with experiments to verify, so as to obtain more information to guide the further design and development of ASSBs.

In addition to the improvement of calculation methods, the improvement of sulfide electrolyte performance is also the key to improve the overall performance of solid-state batteries. At present, the design of composite electrolyte is a good way to be applied and expected to realize industrial production. The polymer with stable performance and wide electrochemical window is combined with sulfide electrolyte to prepare a composite electrolyte with a 3D ion-conducting framework, which can effectively alleviate the interface problems inside the battery. The advantages and disadvantages of sulfide electrolyte systems are very obvious. The development of solid-state lithium batteries in the future still depends on sulfide electrolytes, but more effective strategies are needed to solve the problems in solid-state batteries.

In summary, the research for ASSB is a systematic project and the development of ASSB should be considered as a whole, rather than focusing on a single breakthrough. Foreseeably, with the continuous efforts of scientists and engineers worldwide, commercial SSEs-based ASSBs/SSBs with high safety and high energy densities can be achieved for large applications in the not too distant future.

Declaration of competing interest

The authors declare that they have no known competing financial interests or personal relationships that could have appeared to influence the work reported in this paper.

Acknowledgments

We acknowledge financial support from the National Natural Science Foundation of China (Nos. 52171082 and 51001091) and the Program for Innovative Research Team (in Science and Technology) in University of Henan Province (No. 21IRTSTHN003). This work was also partially supported by the Provincial Scientific Research Program of Henan (No. 182102310815), Nuclear Material Technology Innovation Fund for National Defense Technology Industry (No. ICNM-2021-YZ-02), and the Science and Technology Project of Henan Province (No. 232102241036).

References

[1] O. Geden, Nat. Geosci. 9 (2016) 340–342.
[2] J. Bednar, M. Obersteiner, A. Baklanov, et al., Nature 596 (2021) 377–383.
[3] D. Sheyfer, R.G. Mariano, T. Kawaguchi, et al., Nano Lett. 23 (2023) 1–7.
[4] M. Armand, J.M. Tarascon, Nature 451 (2008) 652–657.
[5] B. Dunn, H. Kamath, J.M. Tarascon, Science 334 (2011) 928–935.
[6] M.M. Thackeray, C. Wolverton, E.D. Isaacs, Energy Environ. Sci. 5 (2012) 7854.
[7] B. Scrosati, J. Hassoun, Y.K. Sun, Energy Environ. Sci. 4 (2011) 3287.
[8] Y. Zhang, T.T. Zuo, J. Popovic, et al., Mater. Today 33 (2020) 56–74.
[9] X.B. Cheng, R. Zhang, C.Z. Zhao, et al., Chem. Rev. 117 (2017) 10403–10473.
[10] W. Xu, J. Wang, F. Ding, X, et al., Energy Environ. Sci. 7 (2014) 513–537.
[11] N. Nitta, F. Wu, J.T. Lee, et al., Mater. Today 18 (2015) 252–264.
[12] K. Takada, Acta Mater. 61 (2013) 759–770.

[13] Y.S. Hu, Nat. Energy 1 (2016) 16042.
[14] J. Janek, W.G. Zeier, Nat. Energy 1 (2016) 16141.
[15] J.W. Choi, D. Aurbach, Nat. Rev. Mater. 1 (2016) 1–16.
[16] D. Lin, Y. Liu, Y. Cui, Nat. Nanotechnol. 12 (2017) 194–206.
[17] D. Wu, L. Chen, H. Li, et al., Prog. Mater. Sci. 139 (2023) 101182.
[18] A. Manthiram, X. Yu, S. Wang, Nat. Rev. Mater. 2 (2017) 1–16.
[19] D.Y. Oh, Y.J. Nam, K.H. Park, et al., Adv. Energy Mater. 5 (2015) 1500865.
[20] T. Ohtomo, A. Hayashi, M. Tatsumisago, et al., J. Power Sources 233 (2013) 231–235.
[21] G. Oh, M. Hirayama, O. Kwon, et al., Chem. Mater. 28 (2016) 2634–2640.
[22] J. Wu, S. Liu, F. Han, et al., Adv. Mater. 33 (2021) e2000751.
[23] A. Jain, Shyue Ping Ong, G. Hautier, et al., APL Mater. 1 (2013) 011002.
[24] A. Jain, K.A. Persson, G. Ceder, et al., APL Mater. 4 (2016) 053102.
[25] J. Lopez, D.G. Mackanic, Y. Cui, et al., Nat. Rev. Mater. 4 (2019) 312–330.
[26] Y. Wang, W.D. Richards, S.P. Ong, et al., Nat. Mater. 14 (2015) 1026–1031.
[27] M. Yang, Y. Yao, M. Chang, et al., Adv. Energy Mater. 13 (2023) 2300962.
[28] F. Mizuno, A. Hayashi, K. Tadanage, et al., Adv. Mater. 17 (2005) 918–921.
[29] N. Kamaya, K. Homma, Y. Yamakawa, et al., Nat. Mater. 10 (2011) 682–686.
[30] Y. Kato, S. Hori, T. Saito, et al., Nat. Energy 1 (2016) 16030.
[31] A. Banerjee, X. Wang, C. Fang, et al., Chem. Rev. 120 (2020) 6878–6933.
[32] E. Umeshbabu, B. Zheng, Y. Yang, Electrochem. Energy Rev. 2 (2019) 199–230.
[33] Y. Chu, Y. Shen, F. Guo, et al., Electrochem. Energy Rev. 3 (2019) 187–219.
[34] H. Wan, L. Cai, F. Han, et al., Small 15 (2019) e1905849.
[35] L. Xu, S. Tang, Y. Cheng, et al., Joule 2 (2018) 1991–2015.
[36] F. Han, Y. Zhu, X. He, et al., Adv. Energy Mater. 6 (2016) 1501590.
[37] K. Takada, N. Ohta, L. Zhang, et al., Solid State Ionics 179 (2008) 1333–1337.
[38] A. Sakuda, A. Hayashi, M. Tatsumisago, Chem. Mater. 22 (2009) 949–956.
[39] Y. Zhu, X. He, Y. Mo, J. Mater. Chem. A 4 (2016) 3253–3266.
[40] J. Haruyama, K. Sodeyama, Y. Tateyama, ACS Appl. Mater. Interfaces 9 (2017) 286–292.
[41] K.J. Kim, M. Balaish, M. Wadaguchi, et al., Adv. Energy Mater. 11 (2020) 2002689.
[42] H. Xu, G. Cao, Y. Shen, et al., Energy Environ. Mater. 5 (2022) 852–864.
[43] Z. Zhang, S. Chen, J. Yang, et al., ACS Appl. Mater. Interfaces 10 (2018) 2556–2565.
[44] X. Rui, D. Ren, X. Liu, et al., Energy Environ. Sci. 16 (2023) 3552–3563.
[45] W. Li, Y.G. Cho, W. Yao, et al., J. Power Sources 473 (2020) 228579.
[46] N. Tanibata, S. Takimoto, K. Nakano, et al., ACS Mater. Lett. 2 (2020) 880–886.
[47] C.W. Wang, F.C. Ren, Y. Zhou, et al., Energy Environ. Sci. 14 (2021) 437–450.
[48] N. Wu, P.H. Chien, Y. Qian, et al., Angew. Chem. Int. Ed. 59 (2020) 4131–4137.
[49] S. Chen, D. Xie, G. Liu, et al., Energy Storage Mater. 14 (2018) 58–74.
[50] D. Cheng, T.A. Wynn, X. Wang, et al., Joule 4 (2020) 2484–2500.
[51] J. Peng, D. Wu, Z. Jiang, et al., ACS Nano 17 (2023) 12706–12722.
[52] S. Zhang, J. Ma, S. Dong, et al., Electrochem. Energy Rev. 6 (2023) 4.
[53] S. Shi, J. Gao, Y. Liu, et al., Chin. Phys. B 25 (2016) 018212.
[54] K.B. Hatzell, X.C. Chen, C.L. Cobb, et al., ACS Energy Lett. 5 (2020) 922–934.
[55] S. Lou, F. Zhang, C. Fu, et al., Adv. Mater. 33 (2021) e2000721.
[56] J. Wu, L. Shen, Z. Zhang, et al., Electrochem. Energy Rev. 4 (2020) 101–135.
[57] G. Xi, M. Xiao, S. Wang, et al., Adv. Funct. Mater. 31 (2020) 2007598.
[58] X. Xu, K.S. Hui, K.N. Hui, et al., Mater. Horiz. 7 (2020) 1246–1278.
[59] S. Randau, D.A. Weber, O. Kötz, et al., Nat. Energy 5 (2020) 259–270.
[60] Q. He, B. Yu, Z. Li, et al., Energy Environ. Mater. 2 (2019) 264–279.
[61] A. Urban, D.H. Seo, G. Ceder, NPJ Comput. Mater. 2 (2016) 2057–3960.
[62] Q. Zhao, S. Stalin, C.Z. Zhao, et al., Nat. Rev. Mater. 5 (2020) 229–252.
[63] T. Famprikis, P. Canepa, J.A. Dawson, et al., Nat. Mater. 18 (2019) 1278–1291.
[64] R. Chen, Q. Li, X. Yu, et al., Chem. Rev. 120 (2020) 6820–6877.
[65] W. Ji, X. Zhang, D. Zheng, et al., Adv. Funct. Mater. 37 (2022) 2202919.
[66] W. Xie, M. Chang, W. Fan, et al., Mater. Chem. Front. 7 (2023) 2844–2850.
[67] Y. Wang, Z. Wang, D. Wu, et al., eScience 2 (2022) 537–545.
[68] P. Lu, L. Liu, S. Wang, et al., Adv. Mater. 33 (2021) e2100921.
[69] J. Peng, D. Wu, H. Li, et al., Battery Energy 2 (2023) 20220059.
[70] Y. Jin, Q. He, G. Liu, et al., Adv. Mater. 35 (2023) e2211047.
[71] A. Pradel, M. Ribes, Solid State Ionics 18 (1986) 351–355.
[72] A. Hayashi, S. Hama, H. Morimoto, et al., J. Am. Ceram. Soc. 84 (2001) 477–479.
[73] R.C. Xu, X.H. Xia, S.H. Li, et al., J. Mater. Chem. A 5 (2017) 6310–6317.
[74] L. Zhou, M.K. Tufail, N. Ahmad, et al., ACS Appl. Mater. Interfaces 13 (2021) 28270–28280.
[75] T. Kaib, S. Haddadpour, M. Kapitein, et al., Chem. Mater. 24 (2012) 2211–2219.
[76] K.H. Park, D.Y. Oh, Y.E. Choi, et al., Adv. Mater. 28 (2016) 1874–1883.
[77] H. Kwak, K.H. Park, D. Han, et al., J. Power Sources 446 (2020) 227338.
[78] R. Iwasaki, S. Hori, R. Kanno, et al., Chem. Mater. 31 (2019) 3694–3699.
[79] P. Bron, S. Johansson, K. Zick, et al., J. Am. Chem. Soc. 135 (2013) 15694–15697.
[80] J.E. Lee, K.H. Park, J.C. Kim, et al., Adv. Mater. 34 (2022) e2200083.
[81] K.H. Kim, S.W. Martin, Chem. Mater. 31 (2019) 3984–3991.
[82] H.J. Deiseroth, J. Maier, K. Weichert, et al., Z. Anorg. Allg. Chem. 637 (2011) 1287–1294.
[83] C. Yu, S. Ganapathy, J. Hageman, et al., ACS Appl. Mater. Interfaces 10 (2018) 33296–33306.
[84] P. Adeli, J.D. Bazak, K.H. Park, et al., Angew. Chem. Int. Ed. 58 (2019) 8681–8686.
[85] Y. Lee, J. Jeong, H.D. Lim, et al., ACS Sustain. Chem. Engin. 9 (2020) 120–128.
[86] J.M. Tarascon, M. Armand, Nature 414 (2001) 359–367.
[87] R. Koerver, W. Zhang, L. de Biasi, et al., Energy Environ. Sci. 11 (2018) 2142–2158.
[88] T. Shi, Y.Q. Zhang, Q. Tu, et al., J. Mater. Chem. A 8 (2020) 17399–17404.
[89] R. Koerver, I. Dursun, T. Leichtweiß, et al., Chem. Mater. 29 (2017) 5574–5582.
[90] S.G. Ling, J. Gao, R.J. Xiao, et al., Chin. Phys. B 25 (2016) 018208.
[91] W. Schnick, J. Luecke, Solid State Ionics 38 (1990) 271–273.
[92] B.A. Boukamp, R.A. Huggins, Mat. Res. Bull. 13 (1978) 23–32.
[93] X. He, Y. Zhu, Y. Mo, Nat. Commun. 8 (2017) 15893.
[94] R. Jalem, Y. Yamamoto, H. Shiiba, et al., Chem. Mater. 25 (2013) 425–430.
[95] Y. Mo, S.P. Ong, G. Ceder, et al., Chem. Mater. 24 (2011) 15–17.
[96] Y. Zhu, X. He, Y. Mo, et al., J. Mater. Chem. A 4 (2016) 3253–3266.
[97] A.V.D. Walle, M. Asta, G. Ceder, Calphad 26 (2002) 539–553.
[98] A.V.D. Walle, G. Ceder, J. Phase Equilibria 23 (2002) 348–359.
[99] W.D. Richards, L.J. Miara, Y. Wang, et al., Chem. Mater. 28 (2015) 266–273.
[100] Y. Zhu, X. He, Y. Mo, ACS Appl. Mater. Interfaces 7 (2015) 23685–23693.
[101] H. Xu, Y. Yu, Z. Wang, et al., Energy Environ. Mater. 2 (2019) 234–250.
[102] H. Xu, W. Xiao, Z. Wang, et al., J. Energy Chem. 59 (2021) 229–241.
[103] W. Zhang, D.A. Weber, H. Weigand, et al., ACS Appl. Mater. Interfaces 9 (2017) 17835–17845.
[104] B.N.J. Persson, Surf. Sci. Rep. 61 (2006) 201–227.
[105] H.K. Tian, Y. Qi, J. Electrochem. Soc. 164 (2017) E3512–E3521.
[106] M. Yamamoto, M. Takahashi, Y. Terauchi, JCS Japan 125 (2017) 391–395.
[107] S. Choi, M. Jeon, J. Ahn, et al., ACS Appl. Mater. Interfaces 10 (2018) 23740–23747.
[108] J. Haruyama, K. Sodeyama, L. Han, et al., Chem. Mater. 26 (2014) 4248–4255.
[109] A.M. Nolan, Y. Liu, Y. Mo, ACS Energy Lett. 4 (2019) 2444–2451.
[110] W.S.K. Bong, A. Shiota, T. Miwa, et al., J. Power Sources 577 (2023) 233259.
[111] L. Peng, H. Ren, J. Zhang, et al., Energy Storage Mater. 43 (2021) 53–61.
[112] X. Li, L. Jin, D. Song, et al., J. Energy Chem. 40 (2020) 39–45.
[113] F. Ren, Z. Liang, W. Zhao, et al., Energy Environ. Sci. 16 (2023) 2579–2590.
[114] Y. Xiao, L.J. Miara, Y. Wang, et al., Joule 3 (2019) 1252–1275.
[115] D. Cao, Y. Zhang, A.M. Nolan, et al., Nano Lett. 20 (2020) 1483–1490.